

M. Latif · K. Sperber · J. Arblaster · P. Braconnot
 D. Chen · A. Colman · U. Cubasch · C. Cooper
 P. Delecluse · D. DeWitt · L. Fairhead · G. Flato
 T. Hogan · M. Ji · M. Kimoto · A. Kitoh · T. Knutson
 H. Le Treut · T. Li · S. Manabe · O. Marti
 C. Mechoso · G. Meehl · S. Power · E. Roeckner
 J. Sirven · L. Terray · A. Vintzileos · R. Vofß
 B. Wang · W. Washington · I. Yoshikawa · J. Yu
 S. Zebiak

ENSIP: the El Niño simulation intercomparison project

Received: 19 April 2000 / Accepted: 17 April 2001

Abstract An ensemble of twenty four coupled ocean-atmosphere models has been compared with respect to their performance in the tropical Pacific. The coupled models span a large portion of the parameter space and differ in many respects. The intercomparison includes TOGA (Tropical Ocean Global Atmosphere)-type models consisting of high-resolution tropical ocean models and coarse-resolution global atmosphere models, coarse-resolution global coupled models, and a few global coupled models with high resolution in the equatorial region in their ocean components. The per-

formance of the annual mean state, the seasonal cycle and the interannual variability are investigated. The primary quantity analysed is sea surface temperature (SST). Additionally, the evolution of interannual heat content variations in the tropical Pacific and the relationship between the interannual SST variations in the equatorial Pacific to fluctuations in the strength of the Indian summer monsoon are investigated. The results can be summarised as follows: almost all models (even those employing flux corrections) still have problems in simulating the SST climatology, although some

M. Latif · E. Roeckner
 Max-Planck-Institut für Meteorologie, Hamburg, Germany

K. Sperber
 Program for Climate Model Diagnosis and Intercomparison, LLNL, Livermore, CA USA

J. Arblaster · G. Meehl · W. Washington
 National Center for Atmospheric Research, Boulder, CO, USA

P. Braconnot · O. Marti
 Laboratoire de Modelisation du Climat et de l'Environnement, Saclay, France

D. Chen · S. Zebiak
 Lamont Doherty Earth Observatory, Palisades, NY, USA

A. Colman · C. Cooper
 UK Meteorological Office, Bracknell, UK

U. Cubasch · R. Vofß
 Deutsches Klimarechenzentrum, Hamburg, Germany

P. Delecluse · J. Sirven
 LODYC-IPSL, Paris, France

D. DeWitt¹
 Center for Ocean-Land-Atmosphere Studies, Calverton, MD, USA

L. Fairhead · H. Le Treut · A. Vintzileos
 Laboratoire de Meteorologie Dynamique, Paris, France

G. Flato
 Canadian Centre for Climate Modelling and Analysis, Victoria, BC, Canada

T. Hogan · T. Li
 Naval Research Laboratory, Monterey, CA, USA

M. Ji
 National Centers for Environment Prediction, Camp Springs, MD, USA

M. Kimoto
 Center for Climate System Research, Tokyo, Japan

A. Kitoh
 Meteorological Research Institute, Tsukuba, Japan

T. Knutson
 Geophysical Fluid Dynamics Laboratory, Princeton, NJ, USA

S. Manabe
 Earth Frontier Research System, Tokyo, Japan

C. Mechoso · J. Yu
 University of California, Los Angeles, CA, USA

S. Power
 Bureau of Meteorology Research Centre, Melbourne, Australia

L. Terray
 CERFACS, Toulouse, France

B. Wang
 University of Hawaii, Honolulu, HI, USA

I. Yoshikawa
 Japan Meteorological Agency, Tokyo, Japan

¹ Also at: Lamont Doherty Earth Observatory, Palisades, NY, USA

improvements are found relative to earlier intercomparison studies. Only a few of the coupled models simulate the El Niño/Southern Oscillation (ENSO) in terms of gross equatorial SST anomalies realistically. In particular, many models overestimate the variability in the western equatorial Pacific and underestimate the SST variability in the east. The evolution of interannual heat content variations is similar to that observed in almost all models. Finally, the majority of the models show a strong connection between ENSO and the strength of the Indian summer monsoon.

1 Introduction

The El Niño/Southern Oscillation (ENSO) phenomenon is the most prominent interannual climate fluctuation in the tropical Pacific (see Philander 1990 for an introduction to ENSO). Although ENSO originates in the tropics, it affects not only regional but also global climate, the ecology of the tropical Pacific and the economies of many countries. ENSO is a classical example of large-scale air-sea interactions and it has become a good test-bed for coupled ocean-atmosphere models. Although ENSO modelling has advanced considerably during the last decade (see the special issue of the *Journal of Geophysical Research* on the TOGA period by Anderson et al. 1998), several aspects of the simulated climatology and ENSO are not well captured by present-day coupled models, as described below.

Here, we present an intercomparison of coupled models that focuses on the simulation of ENSO. However, since the annual mean state and the seasonal cycle in the equatorial Pacific also involve air-sea interactions, and since ENSO is influenced by the underlying background conditions, we also discuss the annual mean state and the seasonal cycle simulated by the coupled models. Furthermore, the response of the tropical climate system to external forcing (such as greenhouse warming) may critically depend on the simulation of the climatology. Tropical feedbacks may even influence the stability of thermohaline circulation, as recently shown by Latif et al. (2000) and Latif (2001). Our intercomparison study is a follow-up of earlier intercomparison studies, namely those of Neelin et al. (1992) who focused on the interannual variability and Mechoso et al. (1995) who concentrated on the simulation of the annual mean state and the seasonal cycle. Here, we investigate also the relationships between equatorial Pacific SST anomalies and upper ocean heat content anomalies and provide correlations between equatorial Pacific SST anomalies and the strength of the Indian summer monsoon.

The models included in our intercomparison cover a large part of the parameter space. Some models are TOGA (Tropical Ocean Global Atmosphere)-type models with high resolution tropical Pacific ocean models coupled to global atmosphere models, while other models are global in both the ocean and the

atmosphere but run at coarse resolution. A few of the global coupled models, however, employ high resolution in the equatorial region. For comparison we include also the intermediate coupled model of Zebiak and Cane (1987), the LAMONT model. Some models are flux-corrected (using either annual mean or monthly varying corrections), others are not, and some models employ anomaly coupling, while one model prescribes the clouds. The models also differ considerably in the vertical and horizontal resolutions. This model diversity makes it difficult to stratify the models, and we therefore decided to refrain from doing so.

This work is a spin-off of the Coupled Model Intercomparison Project (CMIP, Meehl et al. 2000a) and was performed under the auspices of the CLIVAR/GOALS Numerical Experimentation Group (NEG-1, now WGSIP). A companion paper describing the variability in all three tropical oceans (STOIC: Study of Tropical Oceans In Coupled models, also undertaken under the auspices of the CLIVAR-WGSIP) is in preparation. Additionally, AchutaRao and Sperber (2000) analyse other aspects of ENSO variability in the CMIP models. Section 2 provides brief model descriptions. The simulation of the annual mean equatorial Pacific SST is described in Sect. 3, while the simulation of the annual cycle in equatorial Pacific SST is discussed in Sect. 4. Section 5 deals with the simulation of the interannual variability in the equatorial Pacific, while we explore in Sect. 6 the interaction of ENSO with the Indian summer monsoon. A brief summary and discussion of the major findings follows in Sect. 7.

2 Model descriptions

We present only very brief model descriptions. A summary is given in Table 1. The reader is referred to the referenced papers for more information about the coupled models. Some of the coupled models also participated in CMIP, and some additional information on these can be obtained from the relevant Internet page (<http://www-pcmdi.llnl.gov/modeldoc/cmip>). It should be noted that the resolutions correspond to the ocean components and are those used in the equatorial region, which we concentrate on. Some models, such as the DKRZ-OPYC and MPI models, have high oceanic resolution in the equatorial region only. Upper ocean heat content was not provided directly for all models, but alternative measures of upper ocean heat content were given, as indicated in Table 1. Sea level, for instance, is a very good approximation of the upper ocean heat content in the tropical regions. Since we computed correlations only, the choice of the measure of the upper ocean heat content should not have a strong impact on the results. The requested minimum length of the integrations is 20 years, but some groups provided much longer records such as GFDL-R15 and CCC. We provide a brief description of each model. The horizontal resolutions are expressed as degrees longitude/latitude. Please note that some models use enhanced resolution near the equator, which is indicated by giving the range of the meridional resolution used.

BMRC

The coupled model described by Power et al. (1998) is a global climate model. The atmosphere model is a low-order spectral

model run at R21 ($3.2^\circ \times 5.6^\circ$) resolution and with nine vertical levels, while the ocean model is MOM (the GFDL primitive equation model described by Pacanowski 1995) run at a horizontal resolution of $2.0^\circ \times 0.5\text{--}5.9^\circ$ and with 25 vertical levels (Power et al. 1995). The coupled model does not employ flux correction.

Table 1 Models used and some of their characteristics

Model	Eq. resolution in the ocean (longitude, latitude)	Heat content depth range (m)	Flux adjustment	References
(BMRC) Bureau of Meteorology Research Centre Melbourne, Australia	$2^\circ, 0.5^\circ$	300	None	Power et al. (1995, 1998) Pacanowski (1995)
(CCCMA) Canadian Centre for Climate Modelling and Analysis Victoria, BC Canada	$1.8^\circ, 1.8^\circ$	330	Heat, <i>P-E</i>	Flato et al. (2000)
(CCSR) Center for Climate System Research Tokyo, Japan	$2.5^\circ, 0.5^\circ$	360	SST relaxed poleward of 55°N	Kimoto (1998) Watanabe et al. (1998) Kimoto and Shen (1997)
(CEA-DSM SACLAY) Laboratoire de Modelisation du Climat et de l'Environnement Saclay, France	$4^\circ, 1^\circ$	Information pending	None	Braconnot et al. (1997)
(CERFACS) Centre Europeen de Recherche et de Formation Avancee en Calcul Scientifique Toulouse, France	$0.8^\circ, 0.3^\circ$	Depth of 20° isotherm	None	Terray (1998) Delecluse et al. (1993)
COLA Center for Ocean-Land- Atmosphere Studies Calverton, MD USA	$3^\circ, 1^\circ$	375	None	DeWitt and Schneider (1998)
(DKRZ-OPYC) Deutsches Klimarechenzentrum Hamburg, Germany	$2.8^\circ, 0.5^\circ$	350	Heat, <i>P-E</i>	Roeckner et al. (1996) Bacher et al. (1998) Oberhuber (1993)
(DKRZ-LSG) Deutsches Klimarechenzentrum Hamburg, Germany	$4^\circ, 4^\circ$	300	Heat, <i>P-E</i> , momentum	Voss et al. (1998) Timmermann et al. (1998) Maier-Reimer et al. (1993)
(GFDL-R15) Geophysical Fluid Dynamics Laboratory Princeton, NJ USA	$3.8^\circ, 4.5^\circ$	400	Heat, <i>P-E</i>	Manabe et al. (1991) Bryan and Lewis (1979)
(GFDL-R30) Geophysical Fluid Dynamics Laboratory Princeton, NJ USA	$1.9^\circ, 2.2^\circ$	400	Heat, <i>P-E</i>	Knutson and Manabe (1998)
(HAWAII) University of Hawaii Honolulu, HI USA	$2^\circ, 1^\circ$	Thermocline depth	Prescribed cloud	Wang and Fang (1999)
(JMA) Japan Meteorological Agency Tokyo, Japan	$2.5^\circ, 0.5^\circ$	360	None	Yoshikawa et al. (1995) Kimoto et al. (1997)
(LAMONT) Lamont Doherty Earth Observatory Palisades, NY USA	$2.0^\circ, 0.5^\circ$	Sea level	Anomaly coupling	Zebiak and Cane (1987)
(LMD/LODYC-2.5) Laboratoire de Meteorologie Dynamique Paris, France	$0.8^\circ, 0.3^\circ$	350	None	Sirven and Vintzileos (1999) Sirven (1996)
(LMD/LODYC-TOGA) Laboratoire de Meteorologie Dynamique Paris, France	$0.8^\circ, 0.3^\circ$	350	None	Vintzileos et al. (1999a, b)
(LMD/LODYC-GLOBAL) Laboratoire de Meteorologie Dynamique Paris, France	$2^\circ, 0.5^\circ$	364	None	Laurent et al. (1998)
MPI Max-Planck-Institut für Meteorologie Hamburg, Germany	$2.8^\circ, 0.5^\circ$	Sea level	None	Frey et al. (1997) Venzke et al. (2000) Wolff et al. (1996)
MRI Meteorological Research Institute Tsukuba, Japan	$2.5^\circ, 0.5^\circ$	300	Heat, <i>P-E</i>	Yukimoto et al. (1996) Nagai et al. (1992)
NAVAL (NRL) Naval Research Laboratory Monterey, CA USA	$2^\circ, 0.5^\circ$	320	Heat	Li and Hogan (1998)
NCAR-CSM National Center for Atmospheric Research Boulder, CO USA	$2.4^\circ, 1.2^\circ$	353	None	Boville and Gent (1999)

Table 1 Continued

Model	Eq. resolution in the ocean (longitude, latitude)	Heat content depth range (m)	Flux adjustment	References
NCAR-WM National Center for Atmospheric Research Boulder, CO USA	1°, 1°	360	None	Meehl and Washington (1996) Washington and Meehl (1996) Washington et al. (1994)
NCEP National Centers for Environmental Prediction Camp Springs, MD USA	1.5°, 0.3°	360	One-way anomaly coupling	Ji et al. (1998)
UCLA University of California at Los Angeles Los Angeles, CA USA	1°, 0.3°	316	None	Mechoso et al. (1998)
UKMO United Kingdom Meteorological Office Bracknell, UK	1.3°, 1.3°	360	None	Gordon et al. (2000)

CCC

The coupled model described by Flato et al. (2000) is a global climate model. The atmosphere model is a low-order spectral model run at T32 ($3.8^\circ \times 3.8^\circ$) resolution and with ten vertical levels, while the ocean model is MOM run with a horizontal resolution of $1.8^\circ \times 1.8^\circ$ and with 29 vertical levels. The coupled model employs monthly varying flux corrections for heat and fresh water.

CCSR

The coupled model described by Kimoto (2001) and Watanabe et al. (1998) is a global climate model without interactive sea ice. The atmosphere model is a low-order spectral model run at T21 ($5.6^\circ \times 5.6^\circ$) resolution and with 20 vertical levels, while the ocean model described by Kimoto and Shen (1997) is based on the dynamical framework of Bryan (1969) run at a horizontal resolution of $2.5^\circ \times 0.5^\circ$ – 2.0° and with 20 vertical levels. The coupled model does not employ flux correction.

CEA-DSM (SACLAY)

The coupled model described by Braconnot et al. (1997) is a global climate model. The atmosphere model is basically the same model as used in LMD-Global but run at a coarser resolution. It is a gridpoint model with a zonal resolution of 5.6° , 50 latitude gridpoints evenly spaced in the sine of latitude and 11 vertical levels. The ocean model is OPA (the French primitive equation model described by Delecluse et al. 1993) run at a horizontal resolution of $4.0^\circ \times 1.0^\circ$ – 13.0° and with 31 vertical levels. The coupled model does not employ flux corrections.

CERFACS

The coupled model described by Terray (1998) is a TOGA-type model. The atmosphere model is a low-order spectral model run at T42 ($2.8^\circ \times 2.8^\circ$) resolution and with 31 vertical levels, while the ocean model is OPA run at a horizontal resolution of $0.75^\circ \times 0.33^\circ$ – 1.5° and with 28 vertical levels. The coupled model does not employ flux correction.

COLA

The coupled model described by DeWitt and Schneider (1998) is a global climate model. The atmosphere model is a low-order spectral model run at T30 ($3.75^\circ \times 3.75^\circ$) and with 18 vertical levels,

while the ocean model is MOM run at a horizontal resolution of $3.0^\circ \times 1.0^\circ$ – 3.0° and with 20 vertical levels. The coupled model does not employ flux correction.

DKRZ-OPYC

The coupled model described by Roeckner et al. (1996) and Bacher et al. (1998) is a global climate model. The atmosphere model is a low-order spectral model run at T42 ($2.8^\circ \times 2.8^\circ$) resolution and with 19 vertical levels, while the ocean model is OPYC (a primitive equation ocean model formulated in isopycnal coordinates described by Oberhuber (1993)) run at a horizontal resolution of $2.8^\circ \times 0.5^\circ$ – 2.8° and with 11 layers. The coupled model employs annual mean flux corrections for heat and fresh water.

DKRZ-LSG

The coupled model described by Voss et al. (1998) and Timmermann et al. (1998) is a global climate model. The atmosphere model is a low-order spectral model run at T21 ($5.6^\circ \times 5.6^\circ$) resolution and with 19 vertical levels, while the ocean model is LSG (a primitive equation ocean model neglecting the momentum advection described by Maier-Reimer et al. 1993) run at a horizontal resolution of $4.0^\circ \times 4.0^\circ$ and with 11 vertical levels. The coupled model employs monthly varying flux corrections for momentum, heat and fresh water.

GFDL-R15

The coupled model described by Manabe et al. (1991) is a global climate model. The atmosphere model is a low-order spectral model run at R15 ($4.5^\circ \times 7.5^\circ$) resolution and with nine vertical levels, while the ocean model is the original GFDL primitive equation model (Bryan and Lewis 1979) run at a horizontal resolution of $3.8^\circ \times 4.5^\circ$ and with 12 vertical levels. The coupled model employs monthly varying flux corrections for heat and fresh water.

GFDL-R30

The coupled model described by Knutson and Manabe (1998) is similar to the GFDL-R15 model already described. The main difference is the higher resolution. The atmosphere model is run at R30 ($2.25^\circ \times 3.75^\circ$) and with 14 vertical levels, while the ocean model is run at a horizontal resolution of $1.88^\circ \times 2.24^\circ$ and with 18 vertical levels. The coupled model employs monthly varying flux corrections for heat and fresh water.

HAWAII

The coupled model described by Wang and Fang (2000) is a tropical model covering the entire tropics from 30°N–30°S. Realistic coast lines are used but without mass exchange between the Pacific and other ocean basins. Only the tropical Pacific Ocean actively interacts with the atmosphere. The surface temperature outside the tropical Pacific is specified from climatology. Both the atmosphere and ocean models have a resolution of $2^\circ \times 1^\circ$. Both component models are grid point primitive equation models, with 2.5 levels in the vertical. No flux correction is applied, but climatological cloud cover is prescribed from observations.

JMA

The coupled model described by Yoshikawa et al. (1995) is a global climate model without interactive sea ice. The atmosphere model is a low-order spectral model run at T42 ($2.8^\circ \times 2.8^\circ$) resolution and with 21 vertical levels, while the ocean model described by Kimoto et al. (1997) is based on the dynamical framework of Bryan (1969) run at a horizontal resolution of $2.5^\circ \times 0.5\text{--}2.0^\circ$ and with 20 vertical levels. The coupled model does not employ flux correction.

LAMONT

The coupled model described by Zebiak and Cane (1987) is an intermediate coupled model of the tropical Pacific. The atmosphere model is a gridpoint model and has zonal resolution of $5.625^\circ \times 2.0^\circ$. The ocean model is run at a horizontal resolution of $2.0^\circ \times 0.5^\circ$. Both the atmosphere and ocean model are based on shallow water dynamics and carry one baroclinic mode. The Lamont model is an anomaly model, and the climatology is prescribed from observations.

LMD-2.5 layer

The coupled model described by Sirven and Vintzileos (1999) is a TOGA-type model. The atmosphere model is a gridpoint model and has zonal resolution of 5.625° , 50 gridpoints evenly spaced in the sine of latitude and 11 vertical levels. The ocean model described by Sirven (1996) is a 2.5 layer reduced gravity model of the tropical Pacific run at a horizontal resolution of $0.75^\circ \times 0.33\text{--}1.5^\circ$ and with 20 vertical levels. The coupled model does not employ flux corrections.

LMD-TOGA

The coupled model described by Vintzileos et al. (1999a, b) is a TOGA-type model. The atmosphere model is a gridpoint model and has zonal resolution of 5.625° , 50 gridpoints evenly spaced in the sine of latitude and 11 vertical levels, while the ocean model is a tropical Pacific version of OPA run at a horizontal resolution of $0.75^\circ \times 0.33\text{--}1.5^\circ$ and with 28 vertical levels. The coupling is based on the technique of delocalised physics and the coupled model does not employ flux correction.

LMD-GLOBAL

The coupled model described by Laurent et al. (1998) is a global climate model. The atmosphere model is a gridpoint model with a zonal resolution of 3.75° , 72 latitude gridpoints evenly spaced in the sine of latitude and 15 vertical levels. The ocean model is a version of OPA (OPA7G2) run at a horizontal resolution of $2.0^\circ \times 0.5\text{--}1.5^\circ$ and with 31 vertical levels. The coupled model does not employ flux corrections.

MPI

The coupled model described by Frey et al. (1997) and Venzke et al. (2000) is a global climate model without interactive sea ice. The atmosphere model is a low-order spectral model run at T42 ($2.8^\circ \times 2.8^\circ$) resolution and with 19 vertical levels, while the ocean model is HOPE (Hamburg Ocean model in primitive equations described by Wolff et al. 1996) run at a horizontal resolution of $2.8^\circ \times 0.5\text{--}2.8^\circ$ and with 20 vertical levels. The coupled model does not employ flux corrections.

MRI

The coupled model described by Yukimoto et al. (1996) is a global climate model. The atmosphere model is a gridpoint model run at a resolution of $5.0^\circ \times 4.0^\circ$ and with 15 vertical levels, while the ocean model is a primitive equation model described by Nagai et al. (1992) run at a horizontal resolution of $2.5^\circ \times 0.5\text{--}2.0^\circ$ and with 21 vertical levels. The coupled model employs monthly varying flux corrections for heat and fresh water.

NAVAL (NRL)

The coupled model described by Li and Hogan (1999) is a TOGA-type model. The atmosphere model is the NAVAL Operational Global Atmospheric Predictions System (NOGAPS) model run at T39 ($2.8^\circ \times 2.8^\circ$) resolution and with 12 vertical levels, while the ocean model is MOM run at a horizontal resolution of $2.0^\circ \times 0.5\text{--}2.0^\circ$ and 25 vertical levels.

NCAR-CSM

The coupled model described by Boville and Gent (1998) is a global climate model. The atmosphere model is a low-order spectral model run at T42 ($2.8^\circ \times 2.8^\circ$) resolution and with 18 vertical levels, while the ocean model is run at a horizontal resolution of $2.4^\circ \times 1.2^\circ$ and with 45 vertical levels. The coupled model does not employ flux corrections.

NCAR-WM

The coupled model described by Meehl and Washington (1996) and Washington and Meehl (1996) is a global climate model. The atmosphere model is a low-order spectral model run at R15 ($7.5^\circ \times 4.5^\circ$) resolution and with nine vertical levels, while the ocean model is one of the NCAR primitive equation models described by Washington et al. (1994) and run at a horizontal resolution of $1.0^\circ \times 1.0^\circ$ and with 20 vertical levels. The coupled model does not employ flux corrections.

NCEP

The coupled model described by Ji et al. (1998) is a TOGA-type model. The atmosphere model is a low-order spectral model run at T40 ($2.8^\circ \times 2.8^\circ$) resolution and with 18 vertical levels, while the ocean model is a Pacific version of MOM run at a horizontal resolution of $1.5^\circ \times 0.33\text{--}1.0^\circ$ and with 28 vertical levels. The coupling is based on a one-way anomaly coupling, i. e. atmospheric fluxes are coupled only by their anomalies, while the SST is coupled fully.

UCLA

The coupled model described by Mechoso et al. (2000) is a TOGA-type model. The atmosphere model is a gridpoint model run at a horizontal resolution of $5.0^\circ \times 4.0^\circ$ resolution and with 15 vertical levels, while the ocean model is a tropical Pacific version of MOM

run at a horizontal resolution of $1.0^\circ \times 0.33\text{--}3.0^\circ$ and with 27 vertical levels. The coupled model does not employ flux corrections.

UKMO

The coupled model described by Gordon et al. (2000) is a global climate model. The atmosphere model is a gridpoint model run at horizontal resolution of $3.75^\circ \times 2.5^\circ$ and with 19 vertical levels, while the ocean model is a GFDL-type primitive equation model run at a horizontal resolution of $1.25^\circ \times 1.25^\circ$ and with 20 vertical levels. The coupled model does not employ flux corrections.

3 Annual mean SST

We used the first twenty years of the model datasets to compute the annual mean and the seasonal cycle. The full length of the integrations were used in the investigation of the interannual variability. Several authors noted that the climatology in the equatorial Pacific results partly from air-sea interactions (e.g. Neelin and Dijkstra 1995; Dijkstra and Neelin 1995). It is therefore of interest to examine how the coupled models simulate the warm pool-cold tongue structure along the equator. In a recent intercomparison paper Mechoso et al. (1995) discuss the annual mean and seasonal cycle of SST as simulated by several coupled GCMs. Their results are basically confirmed by our study, so that we describe both aspects only briefly. We show the observed and simulated equatorial SSTs (averaged over the region $2^\circ\text{N}\text{--}2^\circ\text{S}$) as function of longitude in Fig. 1, which is similar to the figure presented by Mechoso et al. (1995). Our study confirms their finding that most models have a cold bias (10 models are at least

1°C too cold near 150°W), although there are also some models which are too warm (five models are at least 1°C too warm near 150°W). The range in the simulated SSTs amounts to about 6°C near 150°W . The gradient in the central part of the basin, however, is simulated reasonably well by all models, which was not the case for models utilised in the early 1990s (Neelin et al. 1992). Another feature noted by Mechoso et al. (1995) is also evident in Fig. 1, namely some poor performance near the boundaries. Many models simulate much too warm SSTs near the eastern boundary, which may be related to problems in simulating low-level stratus clouds and resolving the steep orography near the coast and the narrow coastal upwelling. The models perform generally better near the western boundary, although some models also show large SST errors in this region. As expected, flux-corrected models perform generally reasonably well in simulating equatorial Pacific SSTs, although there are a few exceptions. In summary, simulating the correct warm pool-cold tongue structure in the equatorial Pacific is still a challenge for coupled models, and even flux correction does not guarantee a good simulation. The latter is plausible, since small initial errors can be amplified by unstable air-sea interactions in the equatorial Pacific. A few models that run without flux correction, however, simulate the SSTs along the equator relatively successfully.

4 Seasonal cycle of SST

The seasonal cycle of SST in the eastern equatorial Pacific has proven very difficult to simulate by coupled

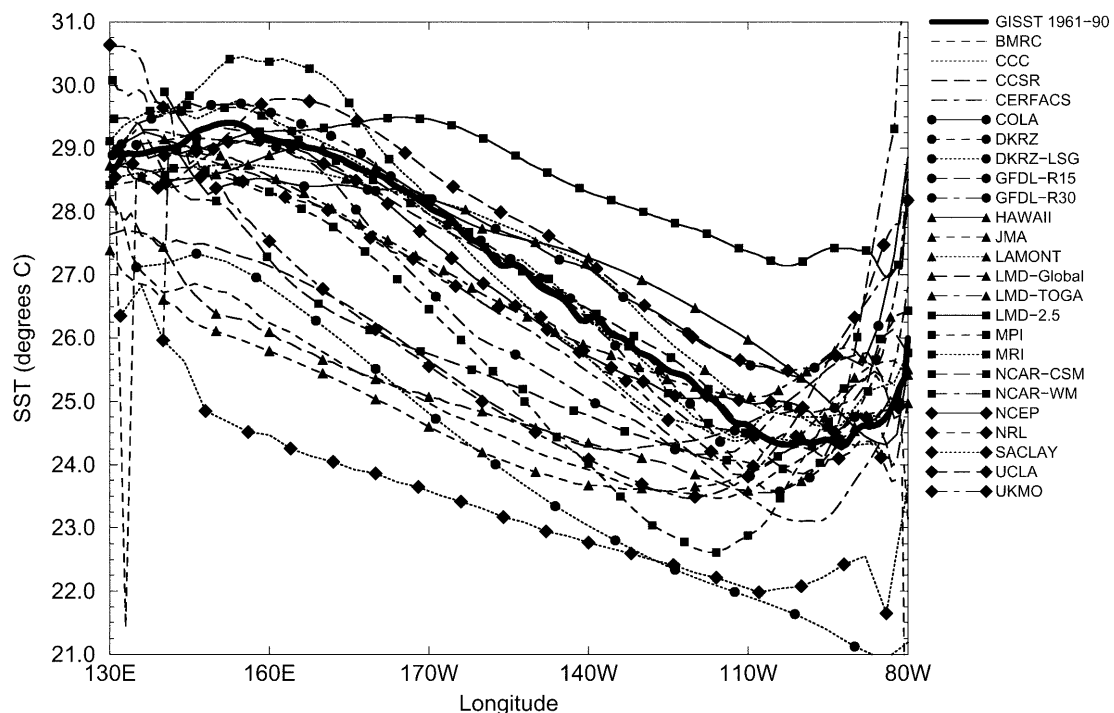


Fig. 1 Simulated and observed annual mean SSTs ($^\circ\text{C}$) along the equator ($2^\circ\text{N}\text{--}2^\circ\text{S}$)

models, as described by Mechoso et al. (1995). Since the Sun crosses the equator twice, one would not necessarily expect the dominant time scale to be annual. As can be inferred from Fig. 2, showing the seasonal cycle in SST (averaged over the region 2°N–2°S) as deviations from the annual mean, the observations indicate a predominance of the annual cycle in the region of the cold tongue in the eastern equatorial Pacific, while a semi-annual cycle is observed in the west. Furthermore, a pronounced westward propagation in the eastern and central equatorial Pacific is found in the observations. Many physical processes both in the ocean and atmosphere and coupled feedbacks contribute to the generation of the annual cycle in the east. One of the main factors controlling the quality of the simulation of the annual cycle is the amount of low-level stratus clouds in the atmosphere models. However, dynamical processes in the ocean and land surface processes are also of great importance in generating the annual cycle. Thus, the annual cycle is a welcome test-case for coupled models, since it involves complex dynamical and physical interactions between the three climate subsystems ocean, atmosphere and land. Please note the annual cycle is prescribed from observations in the LAMONT model.

One of the major findings of our study is that many coupled models appear to still have problems in simulating the annual cycle of the SST in the eastern equatorial Pacific. A summary of the performance is given in Table 2, in which we provide the range of the annual cycle and some specific features of the annual cycle simulations. Many models exhibit a much too weak annual cycle in the eastern Pacific. This is also true for flux-corrected models which were not included in the study by Mechoso et al. (1995). For instance, the GFDL-R15 and DKRZ-LSG models employ both seasonally varying flux corrections, but they fail to simulate a realistic annual cycle. In particular, the amplitude of the annual cycle is much too weak in these two models. This may be related at least partly to the coarse resolution, as demonstrated by the higher-resolution GFDL-R30 model, which simulates a much stronger annual cycle. Other problems that occur are: a too strong annual cycle (e.g. *NAVAL*), a phase shift in the annual cycle (e.g. *BMRC*), the simulation of a semi-annual cycle instead of an annual cycle (e.g. *CEA-DSM*, *NCAR-CSM*), and a westward displacement of the annual cycle (e.g. *NCAR-WM*), standing rather than westward propagating signals (e.g. *COLA*). A few models (*CERFACS*, *HAWAII*, *NCEP*) simulate the SST annual cycle relatively well. All these models employ relatively high meridional resolution (at least 1°) in their ocean components, which indicates strongly that the equatorial and coastal upwellings need to be resolved properly to simulate a realistic annual cycle. However, not all coupled models that employ high resolution in their ocean components simulate a realistic annual cycle (e.g. *DKRZ-OPYC*, *MPI*), which indicates that high resolution is a necessary but not sufficient condition for a good annual cycle simulation. As pointed out by Mechoso

et al. (1995) the quality of the simulation of the low-level stratus clouds is another very important factor. The warm SST biases (Fig. 1) near the eastern boundary simulated by almost all models indicate that the stratus clouds are not well represented in current models.

5 Interannual variability

5.1 SST

5.1.1 Hovmoeller diagrams

We turn now to the overall simulation of equatorial SST, as visualised by longitude-time sections (Hovmöller diagrams) of anomalous SST (Fig. 3) over a 20 year segment. The simulation of the SST anomalies differs in many respects: some models simulate relatively regular ENSO cycles, while other models exhibit a large amount of irregularity. The *CERFACS* model, for instance, simulates very strong interannual variability during the first ten years and much weaker variability during the second ten year period. Some models simulate the strongest variability correctly in the east, while other models incorrectly simulate the strongest variability in the central or western part of the basin. Some models do not simulate much variability at all, while other models simulate too strong variability. Furthermore, the level of high-frequency variability or “noise” is very different between the coupled models.

As pointed out by Neelin et al. (1992) propagation of SST anomalies may point towards the dominance of surface layer processes relative to subsurface processes, while stationary SST anomalies may indicate a dominance of subsurface processes. The latter, which are often associated with wave processes, are important within the “delayed action oscillator” scenario (Schopf and Suarez 1988; Battisti and Hirst 1989) by providing a delayed negative feedback. The Hovmoeller diagrams presented in Fig. 3 may help to identify the propagation characteristics. The observations obtained from the *GISST* dataset show some quite different propagation characteristics, but as shown in many studies (e.g. Latif et al. 1993), the standing component is dominant. As can be inferred from Fig. 3, the distinction between propagating and standing SST anomalies is difficult to realise, especially in models with weak interannual variability. However, one can separate the models roughly into two classes, those which simulate westward propagating and those that simulate standing SST anomalies: fourteen models simulate standing SST anomalies, while ten models simulate westward propagating SST anomalies. Most (eight) of the models simulating westward propagating SST anomalies have a relative coarse-resolution in the meridional direction near the equator, i.e. a north-south resolution of one degree or a coarser resolution. One exception is the *LAMONT* model which employs a resolution of 0.5°.

SST Seasonal Cycle (minus annual mean, 2°N-2°S)

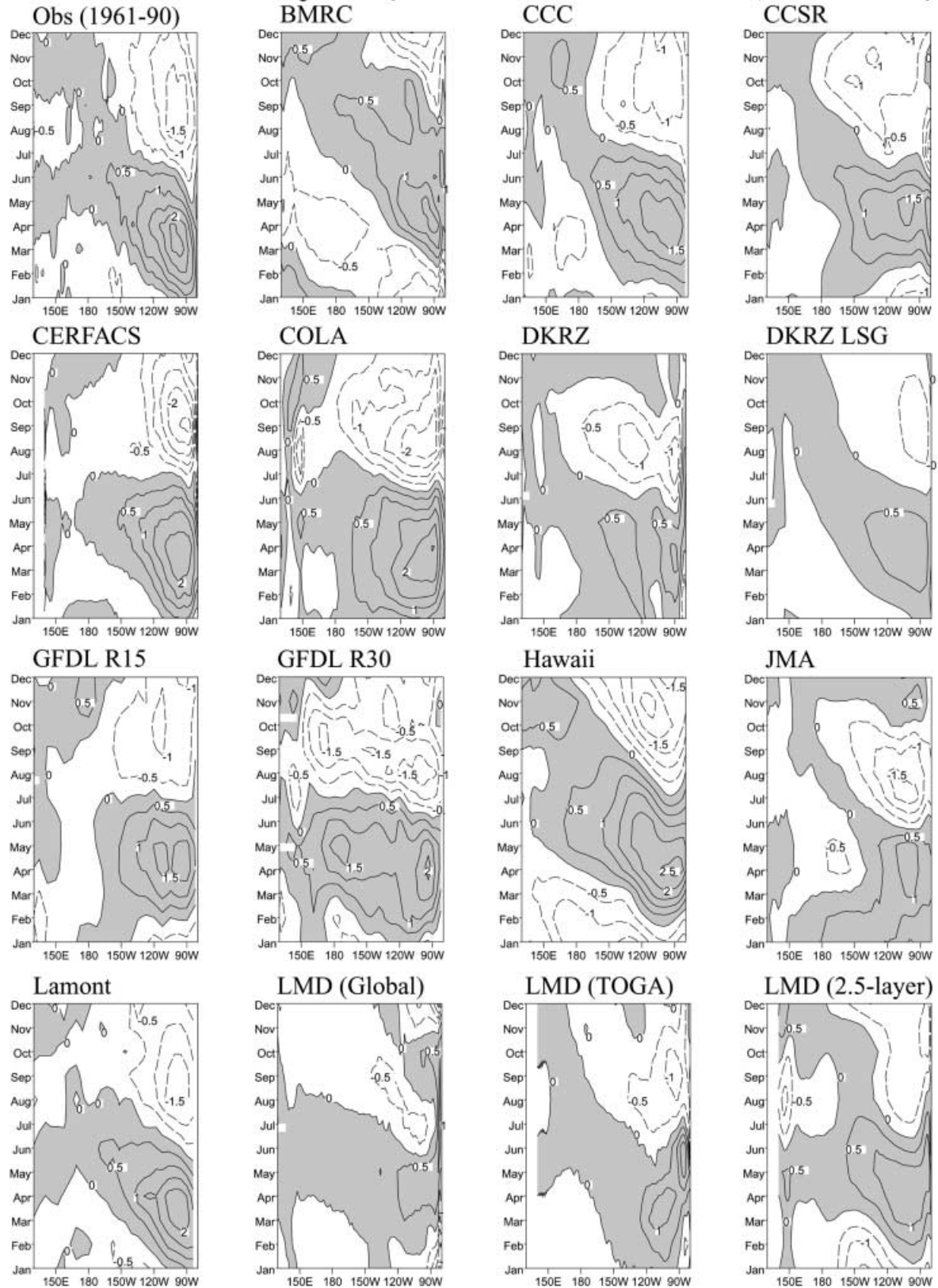


Fig. 2 Simulated and observed SST annual cycle ($^{\circ}\text{C}$) along the equator ($2^{\circ}\text{N}-2^{\circ}\text{S}$). Shown are the deviations from the annual means. Contour interval is 0.5°C and positive values are shaded

SST Seasonal Cycle (minus annual mean, 2°N-2°S)

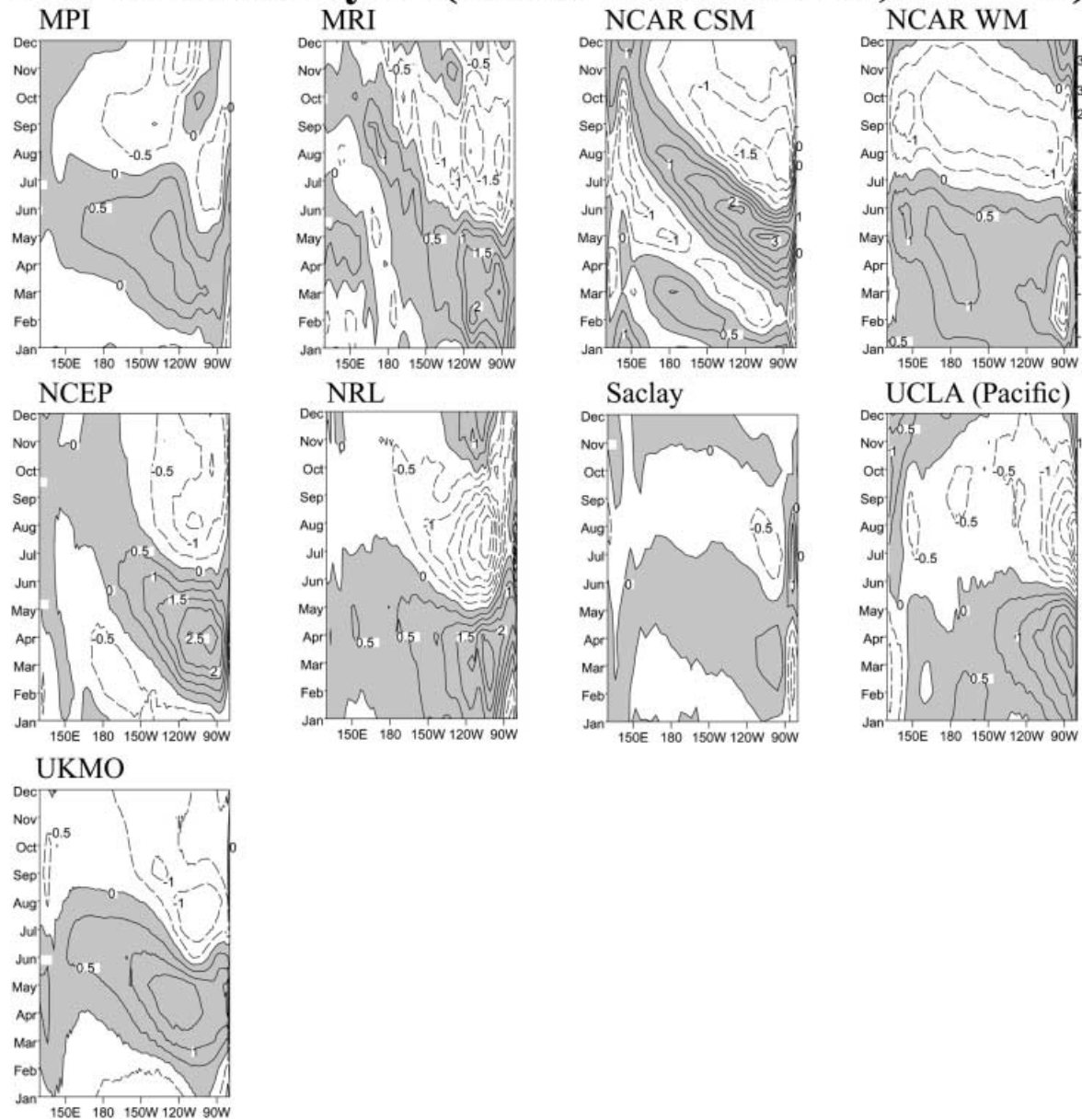


Fig. 2 Continued

Nevertheless, the results indicate that for a realistic simulation of ENSO a meridional resolution higher than one degree is needed. This is confirmed by a visual inspection of the Hovmoeller diagrams: those models that simulate the evolution of the equatorial SST anomalies reasonably well employ meridional resolutions of at least 0.5° in their ocean components.

5.1.2 Niño-3 and Niño-4 indices

The interannual variability simulated by the different coupled models was further analysed by computing in-

dices of equatorial SST anomalies (Table 3). We provide two observational estimates of the Niño-3 index (150°W – 90°W , 5°N – 5°S) and the Niño-4 index (160°E – 150°W , 5°N – 5°S) from the Kaplan et al. (1998) and GISST (Parker et al. 1995) datasets. As can be inferred from the two Niño-3 estimates, there is some uncertainty regarding the strength of the observed interannual variability.

In order to categorise the coupled models, we introduce arbitrary limits for too weak and too strong interannual variability. We consider a model as one that simulates too weak interannual variability, when its standard deviation in the Niño-3 index is less or equal to

Table 2 Simulation of the annual cycle of equatorial SST (2°N–2°S)

Model	Range of annual cycle in the east (°C)	Comments
GISST (obs)	4.0	Annual cycle in the east, semi-annual cycle in the west
BMRC	3.0	Phase shift in the east and the west
CCC	2.5	Too weak annual cycle in the east
CSSR	2.5	Too weak annual cycle in the east
CEA-DSM SACLAY	1.0	Too weak annual cycle in the east
CERFACS	4.5	Realistic
COLA	4.0	No westward phase propagation
DKRZ-OPYC	1.5	Too weak annual cycle in the east
DKRZ-LSG	1.0	Too weak annual cycle in the east
GFDL-R15	1.5	Too weak annual cycle in the east
GFDL-R30	3.5	Annual cycle extends too far to the west
HAWAII	5.0	Too strong annual cycle
JMA	2.5	Too weak annual cycle in the east
LAMONT		Annual cycle prescribed
LMD/LODYC-2.5	1.5	Too weak annual cycle in the east
LMD/LODYC-TOGA	2.0	Too weak annual cycle in the east
LMD/LODYC-GLOBAL		Semi-annual cycle
MPI	2.5	Too weak annual cycle in the east
MRI	4.0	Annual cycle extends too far to the west
NAVAL (NRL)	6.0	Too strong annual cycle
NCAR-CSM		Semi-annual cycle
NCAR-WM	2.0	Annual cycle extends too far to the west
NCEP	4.0	Too weak semi-annual cycle in the west
UCLA	6.0	Too strong annual cycle near the east coast
UKMO	2.5	Too weak annual cycle in the east

0.5 °C, while a model is considered to exhibit too strong variability, when its standard deviation in the Niño-3 index is greater or equal to 1.0 °C. According to these limits, about half of the models (11) are characterised by too weak interannual variability. We note, however, that the range of interannual variability is still relatively large within the “weak-variability” category: we found models with almost no discernible variability (e.g. CCC) and models with obvious variability (e.g. GFDL-R15), as can be inferred also from Fig. 3. Four models simulate too strong variability, while nine models are realistic given our weak/strong threshold. We note, however, that the strength of the interannual SST variability may vary from decade to decade and from century to century, as discussed by Latif (1998). As shown in his Fig. 2, the LAMONT model, for instance, which exhibits the strongest variability in our intercomparison, undergoes very strong interdecadal and centennial variability in the strength of its interannual SST variability.

The coupled models simulate a wide range of behaviours also with respect to the Niño-4 index. We define again limits for a “realistic” simulation: a model is considered to have too weak variability in the Niño-4 region, if its standard deviation is less or equal to 0.3 °C, while a model is considered to have too strong variability if its standard deviation is equal or greater than 0.7 °C. Seven coupled models underestimate the variability in the Niño-4 region, while three models simulate too strong variability, and fourteen models are “realistic”. However, the SST variability in eight models is stronger in the western relative to the eastern equatorial

Pacific, and the variabilities in the two regions are about the same in ten models (see also Fig. 3), which is highly unrealistic. This problem may be related to the cold tongue problem shown in Fig. 1. Thus, the correct simulation of the interannual SST variability appears still to be a problem in most coupled models. There are only five coupled models (CCSR, COLA, DKRZ-OPYC, MPI, UCLA) which simulate the SST variability (as expressed by the two indices) realistically. However, there are other problems in the simulation of the interannual variability, which are also found in these models, as shown below. We note also that a realistic simulation of the strength of the interannual SST variability does not depend on a realistic SST annual cycle simulation, since all the five models mentioned show some deficiencies in their annual cycle simulations (see Table 2). This result is consistent with the findings of Meehl et al. (2000b).

5.1.3 Phase locking to the annual cycle

We analysed next the phase locking of the simulated ENSO variability to the annual cycle. In order to investigate the phase locking, we computed the standard deviations of the simulated Niño-3 SST anomalies as a function of the calendar month (Fig. 4). The observations (GISST) show the well-known dependence of the eastern equatorial SST variability on the annual cycle, with weakest variability in April and strongest variability in December. Fifteen models show almost no detectable phase locking to the annual cycle, and all of

SST (minus seasonal cycle, 2°N-2°S)

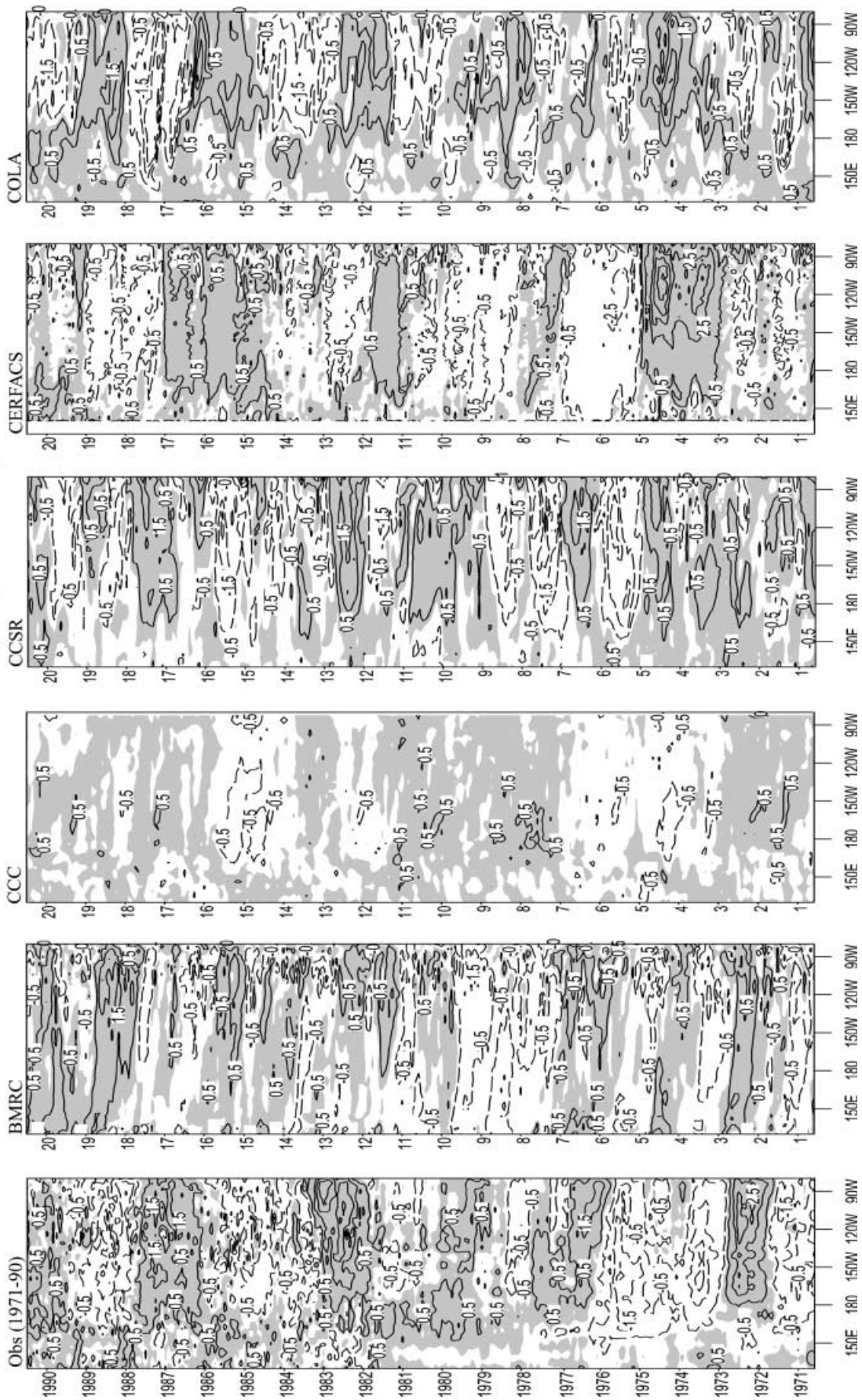


Fig. 3 Hovmöller diagrams of observed and simulated SST anomalies (°C) along the equator (2°N-2°S). Anomalies are defined as departures from the annual cycle. Contour interval is 0.5 °C and positive values are shaded

SST (minus seasonal cycle, 2°N-2°S)

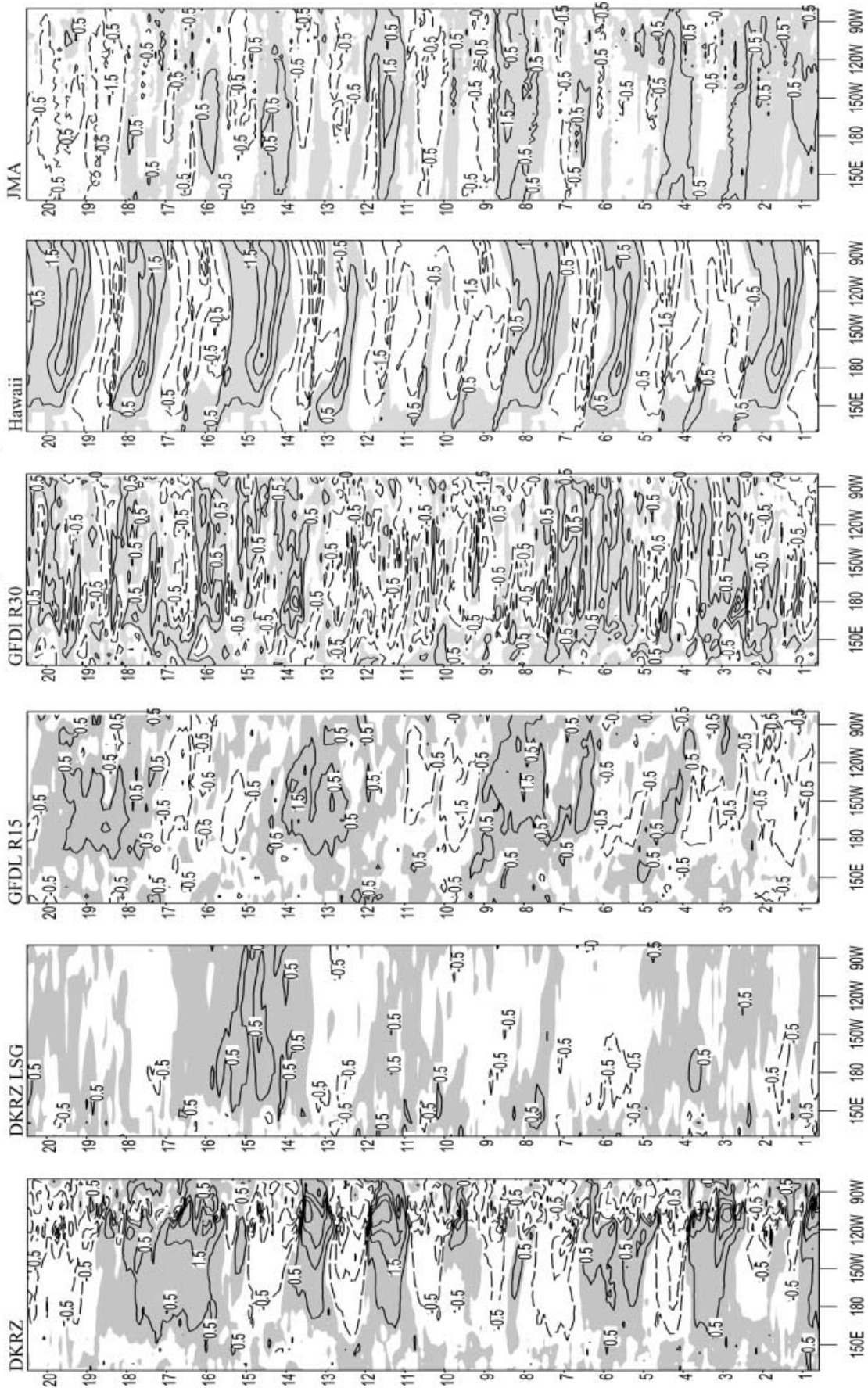


Fig. 3 Continued

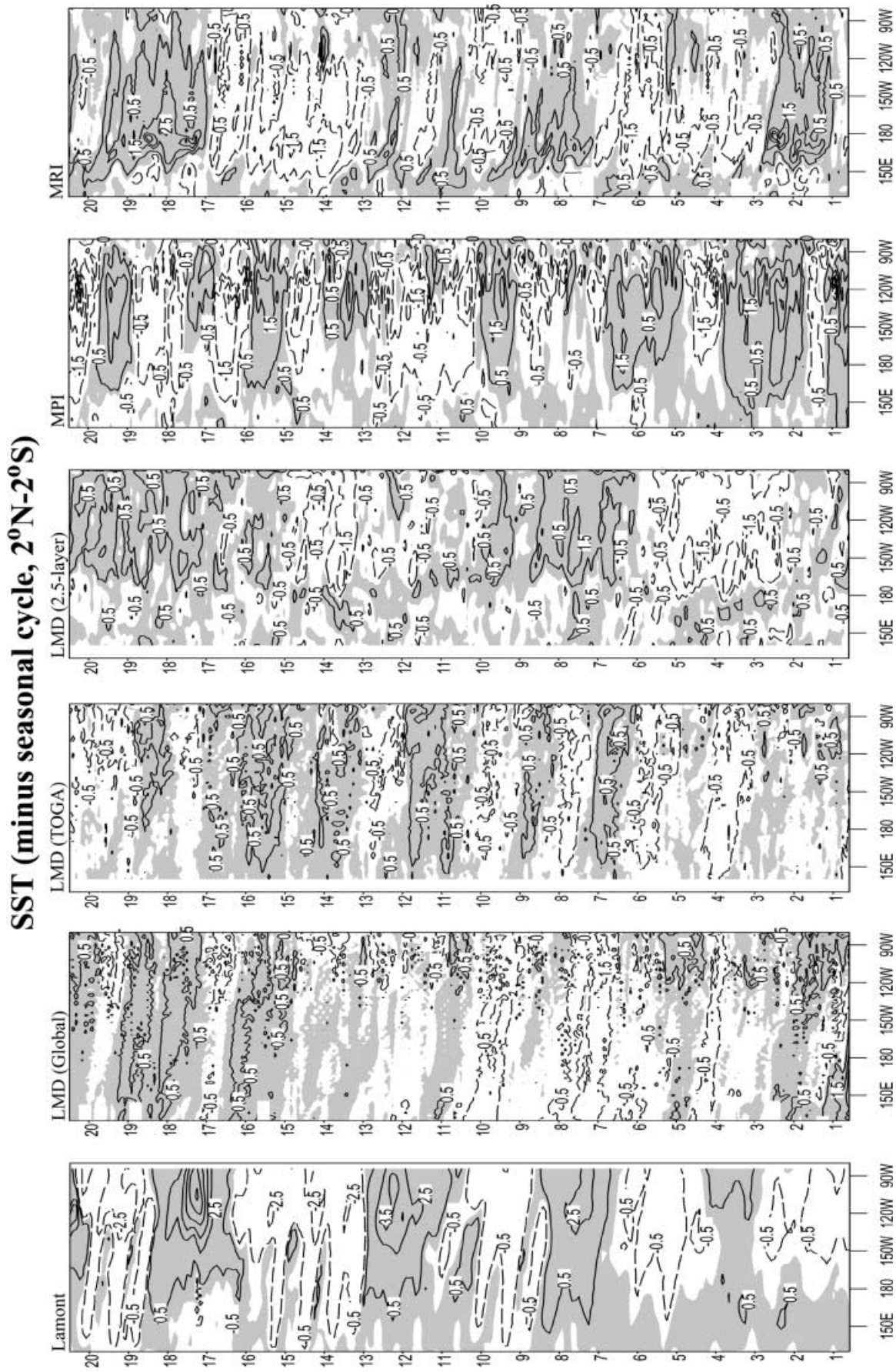


Fig. 3 Continued

SST (minus seasonal cycle, 2°N-2°S)

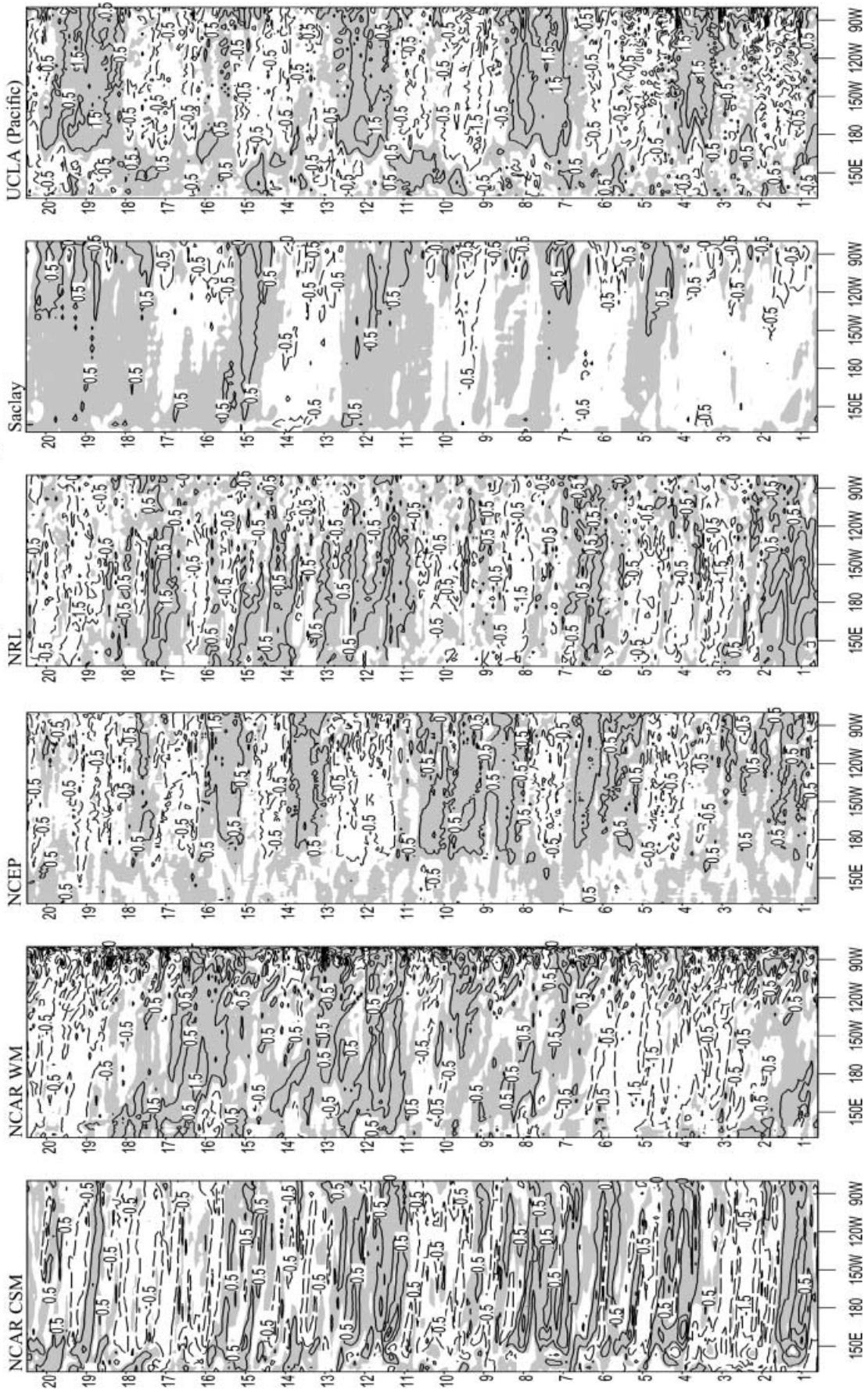


Fig. 3 Continued

SST (minus seasonal cycle, 2°N-2°S)

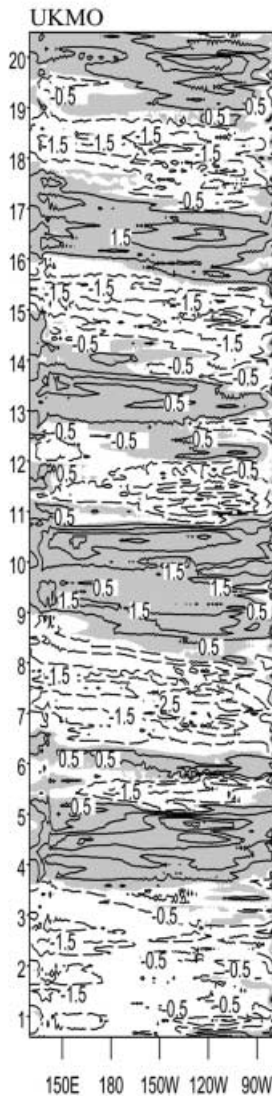


Fig. 3 Continued

these models are characterised by an overall weak variability. Two models (COLA, UCLA) simulate strongest variability in summer, while another model (UKMO) simulates two variability maxima. Another two models (HAWAII, LAMONT) simulate the strongest variability in fall. Only four models (CERFACS, CSSR, DKRZ-OPYC, MPI) simulate the phase locking to the annual cycle reasonably well. Out of these four models, only CERFACS simulates a realistic annual cycle. Thus, there does not exist a systematic relationship between the success of simulating a realistic annual cycle and the simulation of the correct ENSO annual cycle-phase locking.

In summary, the simulation of the interannual SST variability is far from being perfect in most coupled models analysed, even if one considers gross SST indices. Thus, there is substantial potential for model im-

Table 3 Simulated standard deviations of the Niño-3 and Niño-4 SST anomalies

Model	Niño-3 (°C)	Niño-4 (°C)
BMRC	0.4	0.4
CCC	0.2	0.3
CSSR	0.8	0.6
CEA-DSM SACLAY	0.3	0.2
CERFACS	1.0	0.6
COLA	0.7	0.5
DKRZ-OPYC	0.8	0.5
DKRZ-LSG	0.2	0.3
GFDL-R15	0.5	0.4
GFDL-R30	0.4	0.6
HAWAII	1.0	1.0
JMA	0.3	0.4
LAMONT	1.4	0.6
LMD/LODYC-2.5	0.5	0.2
LMD/LODYC-TOGA	0.3	0.3
LMD/LODYC-GLOBAL	0.4	0.3
MPI	0.8	0.6
MRI	0.4	0.7
NAVAL (NRL)	0.3	0.6
NCAR-CSM	0.5	0.5
NCAR-WM	0.5	0.4
NCEP	0.4	0.3
UCLA	0.6	0.4
UKMO	1.1	1.0
OBS (GISST)	0.7	0.5
OBS (KAPLAN)	0.8	0.6

provement, as can be seen from this simple observation/model comparison.

5.2 SST versus τ^x

The zonal wind stress component τ^x is the most important forcing function for equatorial oceans. In particular, the spatial phase relationship between the zonal wind stress and SST anomalies is one important aspect in determining the type of interannual variability simulated. We investigated the relationship between the zonal wind stress anomalies in the western Pacific (Niño-4 region) and the SST anomalies in the eastern Pacific (Niño-3 region) by computing the linear regression coefficient between the two quantities (Table 4). We provide the SST/ τ^x regression derived from the observations (COADS dataset) for comparison. It should be noted that some models may not simulate the wind stress anomalies in the correct place (e.g. too far east), so that the regression may be rather weak. In other models, especially the coarse-resolution models, the SST variability is relatively weak, which could lead to a too large regression coefficient. We found a large range of regression coefficients, with values between 0.001 (N/m²)/°C (CCC, NCAR-WM) and 0.016 (N/m²)/°C (DKRZ-LSG). Only six models (BMRC, GFDL-R30, LAMONT, LMD-TOGA, MPI, UKMO) are within 20% of the value derived from COADS. Interesting is the comparison between the two coarse-resolution global models DKRZ-LSG and GFDL-R15, which

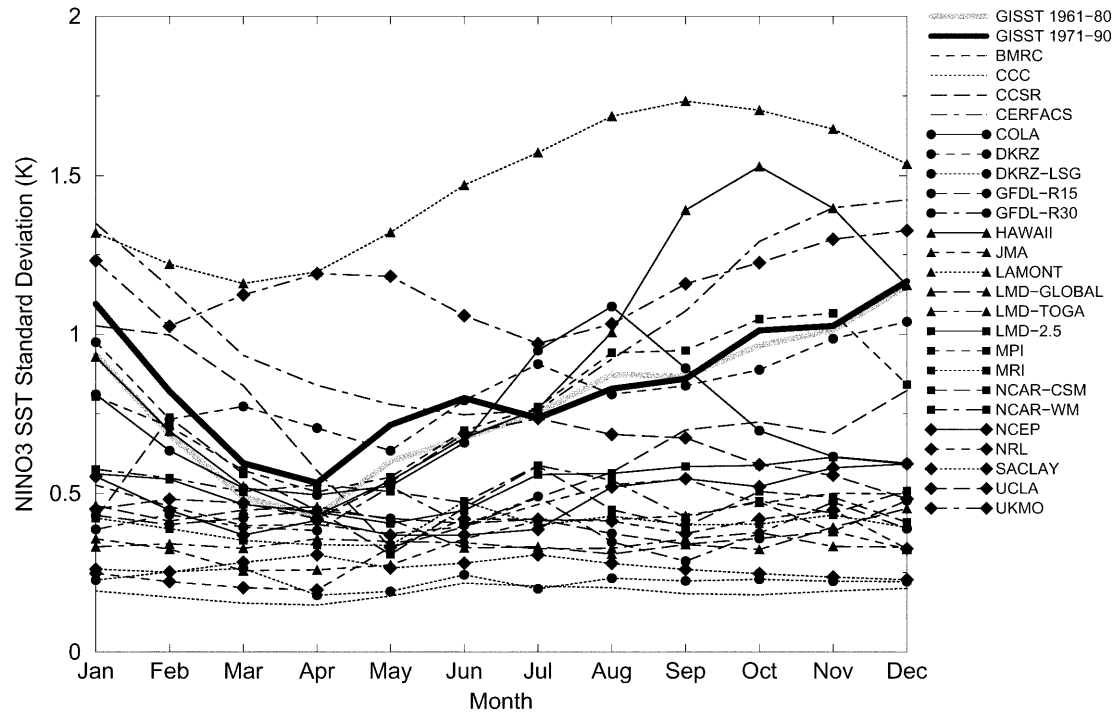


Fig. 4 Observed and simulated standard deviations of the Niño-3 SST anomalies ($^{\circ}\text{C}$) as function of the calendar month

Table 4 Simulated regression coefficients between zonal wind stress anomalies in the Niño-4 region and SST anomalies in the Niño-3 region

Model	Regression [$(\text{N}/\text{m}^2)/^{\circ}\text{C}$]
BMRC	0.007
CCC	0.015
CCSR	0.003
CEA-DSM SCALAY	0.006
CERFACS	0.001
COLA	0.006
DKRZ-OPYC	0.012
DKRZ-LSG	0.016
GFDL-R15	0.003
GFDL-R30	0.007
HAWAII	0.006
JMA	0.005
LAMONT	0.011
LMD/LODYC-2.5	0.013
LMD/LODYC-TOGA	0.009
LMD/LODYC-GLOBAL	0.002
MPI	0.007
MRI	0.014
NAVAL (NRL)	Stress not available
NCAR-CSM	0.005
NCAR-WM	0.001
NCEP	0.015
UCLA	0.005
UKMO	0.008
OBS (COADS)	0.009

yield very different regression coefficients. In the case of the DKRZ-LSG model, it is likely that the weak SST variability (see Table 3) leads to the rather large regression coefficient. The GFDL-R15, on the other hand,

is also characterised by relatively weak SST variability but yields a small regression coefficient. The reason is probably that the GFDL-R15 model simulates westward propagating SST (see Fig. 3) and zonal wind stress anomalies (not shown), which destroys the regression. It is beyond our scope to discuss the failures of the models in further detail. It is, however, obvious that many models do not simulate the correct relationship between the zonal wind stress anomalies in the western equatorial Pacific and the SST anomalies in the eastern equatorial Pacific.

5.3 SST versus heat content

As known from ENSO theory (e.g. Neelin et al. 1994), the subsurface memory of the equatorial ocean is an important component in the ENSO mechanism. In order to compare the subsurface behaviour of the coupled models, we computed correlations between eastern equatorial (Niño-3) SST anomalies and upper ocean heat content as function of longitude along the equator and time lag (Fig. 5). The observed heat contents were obtained from the dataset of White (1995). The eastern equatorial SST anomalies are highly correlated with the upper ocean content anomalies at zero lag in the eastern part of the basin. This reflects the fact that the eastern equatorial SST anomalies are strongly linked to perturbations in the local thermocline depth. The temporal evolution of upper ocean heat content in the observations is characterised by a slow eastward propagation of the anomalies from the western Pacific to the eastern Pacific, which is consistent with the delayed action oscillator scenario. We note, however, that the propaga-

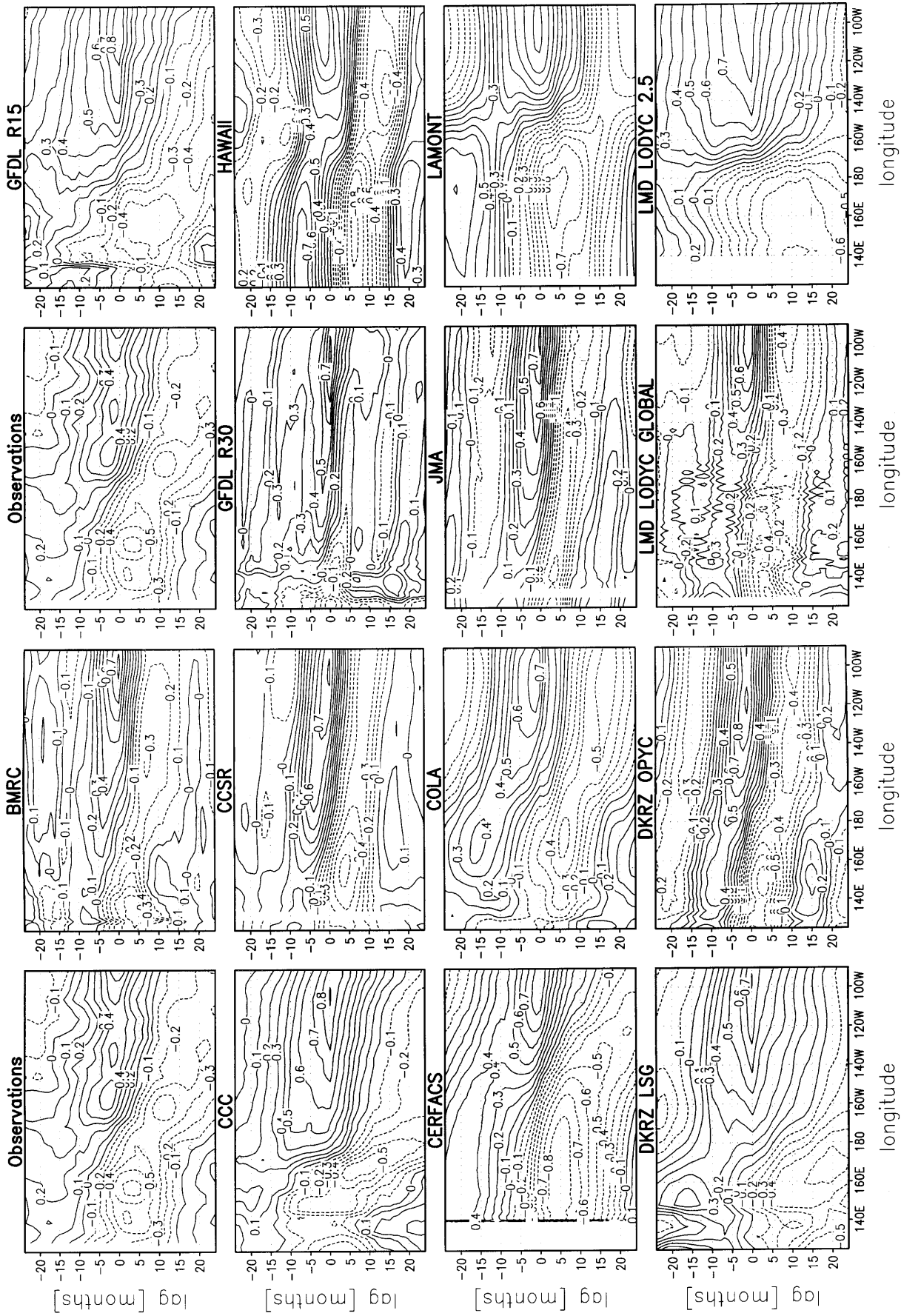


Fig. 5 Correlations of the observed and simulated Niño-3 SST anomalies with the heat content anomalies as function of the longitude along the equator and time lag (month). Contour interval is 0

tion speed is considerably smaller than that expected from the free wave speed of the first baroclinic mode, which is likely due to the fact that the ocean response to low-frequency forcing involves many wave modes that are superimposed on each other (Cane and Sarachik 1981). Furthermore, the observations indicate an oscillatory behaviour with a main period of approximately four years, which has been confirmed by analysing longer datasets.

Almost all models reproduce the high zero-lag correlation between eastern equatorial SST and upper ocean heat content anomalies. Only one model (NCAR-WM) fails to reproduce this relationship, exhibiting only a correlation of about 0.3 in a relatively small region. Furthermore, almost all models show some indications of eastward propagation in the heat content. Thus, at least this important aspect of the interannual variability is simulated well by almost all models. The only exception is again the NCAR-WM model. However, the simulations differ in many respects. The periods are rather different within the ensemble of models, ranging from about two years (seven models) to longer than four years (three models), while oscillatory behaviour is hardly detectable at all in four models. In some models the propagation is too fast or too slow, which is reflected in the different oscillation periods. The region of the most pronounced propagation is also different to that observed in many simulations. This was expected, since most models fail to simulate the correct spatial relationship between western equatorial zonal wind stress and eastern equatorial SST anomalies (see Table 4). It is likely that the position of the zonal wind stress anomalies will determine the region of the most pronounced propagation in the heat content.

We note another model shortcoming. Many models (10) simulate a quite strong anti-correlation in the eastern equatorial Pacific at lags of about 10–20 months. Although the observations reveal an anti-correlation at these time lags, indicating the oscillatory nature of ENSO, many models overestimate this anti-correlation considerably (CERFACS, COLA, DKRZ-OPYC, GFDL-R15, HAWAII, JMA, LAMONT, MPI, UCLA, UKMO). Thus, the variability in these models is too regular, although the reason for this is unclear. One problem may be a too low noise level in the atmospheric component, which may lead to too regular behaviour in SST as shown by Eckert and Latif (1997). Another potential problem may be related to the phase locking of ENSO to the annual cycle, as discussed, for instance, by Chang et al. (1994). They show that depending on the strength of the annual cycle a simulation may be in a chaotic or strongly phase-locked regime.

Interestingly, two of the coarse-resolution global climate models (DKRZ-LSG and GFDL-R15) show a quite realistic heat content evolution. As shown, these two models simulate too weak SST variability, but they simulate the space-time structure of upper ocean heat content much better than some high-resolution models. The GFDL-R15 model, for instance, reproduces the

evolution of upper ocean heat content relatively successfully. This result is surprising, but it indicates that the net effect of the equatorial wave propagation is somehow included in the coarse-resolution models, although these models cannot resolve the waves properly. Thus, some part of the ENSO dynamics seems to be not necessarily distorted in coarse-resolution models.

5.4 Monsoon teleconnections

The last question that we address is the relationship between the equatorial Pacific SST anomalies and the strength of the Indian summer monsoon. We collected two monsoon indices from the coupled models, one dynamical monsoon index (DMI) and one rainfall index (MRI). The DMI is a wind shear index defined by Webster and Yang (1992), while the MRI is based on the rainfall averaged over the region 70°E–100°E and 10°N–25°N. Both indices are averaged over the four months June–September. Monsoon indices were not available from six coupled models (BMRC, HAWAII, LAMONT, NAVAL, NCEP, UKMO). The correlations between both the Niño-3 and Niño-4 SST indices and the two monsoon indices are given in Table 5. The observational estimates are taken from Sperber et al. (2000) who used the NCEP reanalysis to calculate the DMI and observed Indian MRI. Another observational estimate of the Niño-3/MRI correlation for the period 1871–1994 is given by Slingo (1999) and amounts to -0.57 .

There is a general tendency for most models to simulate an out-of-phase relationship between equatorial Pacific SST anomalies and the monsoon indices. Regarding the correlations between the equatorial SST anomalies and the two monsoon indices we note the following additional points: most models simulate stronger SST/monsoon correlations if DMI is used rather than MRI. There are only two exceptions (CERFACS, SACLAY) with respect to Niño-3 and three exceptions (CERFACS, CSSR, NCAR-WM) with respect to Niño-4. Eleven models exhibit correlations of Niño-3 SSTA with DMI larger than 0.25, while eight models exhibit correlations of Niño-3 SSTA with MRI larger than 0.25. Thirteen models exhibit correlations of Niño-4 SSTA with DMI larger than 0.25, while seven models exhibit correlations of Niño-3 SSTA with MRI larger than 0.25. Thus, most models simulate a rather strong connection between the equatorial Pacific SST anomalies and the strength of the Indian summer monsoon. This relationship is more pronounced when a monsoon circulation index (DMI) is used and less pronounced when a rainfall index (MRI) is used. This is consistent with the findings of Sperber and Palmer (1996) who found that the AMIP models were more adept at simulating the DMI as opposed to MRI. Overall, the ensemble of coupled models implies a quite consistent ENSO/monsoon relationship that is found also in the observations. We note, however, that the ENSO/monsoon correlations may undergo substantial

Table 5 ENSO/monsoon teleconnections as expressed by correlations between equatorial Pacific SST anomalies (Niño-3 and Niño-4 SST) and a rainfall (MRI) and a dynamical (DMI) monsoon index

Institute	Niño-3/ MRI	Niño-3/ DMI	Niño-4/ MRI	Niño-4/ DMI	Niño-3/ Niño-4
BMRC					0.85
CCC	-0.05	-0.41	-0.08	-0.38	0.88
CSSR	-0.17	-0.27	-0.23	-0.09	0.80
CEA-DSM SACLAY	0.11	-0.06	0.20	0.01	0.49
CERFACS	-0.64	-0.12	-0.78	-0.24	0.87
COLA	-0.48	-0.81	-0.16	-0.47	0.72
DKRZ-OPYC	-0.51	-0.77	-0.45	-0.63	0.89
DKRZ-LSG	-0.17	-0.60	-0.06	-0.57	0.87
GFDL-R15	-0.14	-0.52	-0.21	-0.37	0.76
GFDL-R30	0.23	-0.33	-0.09	-0.29	0.62
HAWAII					0.53
JMA	-0.09	0.04	0.00	0.17	0.83
LAMONT					0.88
LMD/LODYC-2.5	-0.37	-0.18	-0.01	-0.02	0.41
LMD/LODYC-TOGA	-0.22	-0.09	-0.19	-0.25	0.42
LMD/LODYC-GLOBAL	0.00	-0.10	-0.03	0.35	0.54
MPI	-0.44	-0.60	-0.45	-0.51	0.80
MRI	-0.09	-0.53	-0.30	-0.36	0.85
NAVAL (NRL)					0.95
NCAR-CSM	-0.37	-0.67	-0.57	-0.64	0.81
NCAR-WM	-0.30	-0.06	-0.31	-0.13	0.90
NCEP					0.89
UCLA	-0.40	-0.73	-0.38	-0.65	0.89
UKMO					0.87
Observations	-0.46	-0.58	-0.39	-0.34	0.70

interdecadal variations, as shown in the observational paper by Kumar et al. (1999).

6 Summary and discussion

We have intercompared an ensemble of 24 coupled models with respect to their performance in the equatorial Pacific region. Our study concentrates on the interannual variability, but we investigated also aspects of the climatologies simulated. The following conclusions can be drawn:

1. Many models have still problems in simulating the climatology in the equatorial Pacific. Both the simulated annual mean SSTs and the SST annual cycles can be seriously flawed in the models.
2. Only a few coupled models simulate the interannual SST variability in the equatorial Pacific reasonably well. No model has been found that simulates realistically all aspects of the interannual SST variability considered. Only five models simulate the level of the interannual SST variability, as expressed by the Niño-3 and Niño-4 indices, realistically, while only four models simulate a realistic phase locking of ENSO to the annual cycle. Only three models simulate both aspects of the interannual variability (strength and phase locking) realistically.
3. Most coupled models show a quite strong connection between the equatorial Pacific SST anomalies and the strength of the Indian summer monsoon.

Another interesting result that emerged from this study is that the quality of simulating the climatology does not

necessarily determine the quality of simulating the interannual variability. The strength of the interannual variability can be simulated realistically, even when the climatology is simulated less successfully. Likewise, the phase locking of ENSO to the annual cycle can be simulated reasonably well in a few models despite large errors in the simulation of the annual cycle.

We tried to assess the performance of the coupled models in a rather critical way. The equatorial Pacific is a key region which affects many regions on the globe and which may also be of great importance within the framework of global change. If, for instance, the mean state of the equatorial Pacific and/or the ENSO statistics will change in response to global warming, this will have severe impacts on the climates of many regions. Likewise, the equatorial Pacific is a key region for seasonal forecasting. However, as we have shown, many models are seriously flawed with respect to the simulation of both the climatology and the interannual variability, and it is likely that these errors will affect the ENSO forecast skill. Resolution is one important factor controlling the quality of the simulations, but high resolution, especially the meridional one, is not sufficient to guarantee a good simulation. Thus, there appears to be a large potential to improve the coupled models, even if very basic diagnostics are considered. In conclusion, coupled model development and improvement are still major issues. Both simulations concerning anthropogenic climate change and short-range climate forecasts will benefit from those improvements.

Acknowledgements Dr. K. R. Sperber was supported under the auspices of the US Department of Energy by University of Cali-

ifornia Lawrence Livermore National Laboratory under contract W-7405-Eng-48. The authors would like to thank Mr. Gunnar Hildebrand for his programming assistance. This work was sponsored by the European Union's SINTEX programme.

References

- Achuta Rao et al (2000) El Niño Southern Oscillation in Coupled GCMs PCMDI Report No. 61. Available from PCMDI, LLNL, University of California, Livermore, CA 94550, USA, 46 pp
- Anderson DLT, Sarachik ES, Webster PJ, Rothstein LM (1998) The TOGA Decade. *J Geophys Res* (special issue) 14 167–14 510
- Bacher A, Oberhuber JM, Roeckner E (1998) ENSO dynamics and seasonal cycle in the tropical Pacific as simulated by the EC-HAM4/OPYC3 coupled general circulation model. *Clim Dyn* 14: 431–450
- Battisti DS, Hirst AC (1989) Interannual variability in the tropical atmosphere/ocean system: influence of the basic state, ocean geometry and nonlinearity. *J Atmos Sci* 46: 1687–1712
- Boville BA, Gent PR (1998) The NCAR climate system model, version one. *J Clim* 11: 1115–1130
- Braconnot P, Marti O, Joussaume S (1997) Adjustment and feedbacks in a global coupled ocean-atmosphere model. *Clim Dyn* 13: 507–519
- Bryan K (1969) A numerical method for the study of the circulation of the ocean. *J Comput Phys* 4: 347–376
- Bryan K, Lewis LJ (1979) A water mass model of the world ocean. *J Geophys Res* 84: 2503–2517
- Cane MA, Sarachik ES (1981) The response of a linear baroclinic equatorial ocean to periodic forcing. *J Mar Res* 39: 651–693
- Chang P, Wang B, Li T, Ji L (1994) Interactions between the seasonal cycle and the southern oscillation – frequency entrainment and chaos in a coupled ocean-atmosphere model. *Geophys Res Lett* 21: 817–820
- Delecluse P, Madec G, Imbard M, Levy C (1993) OPA version 7 ocean general circulation model reference manual. LODYC. Internal Report 93/ 05, pp 60
- DeWitt DG, Schneider EK (1998) On the processes determining the annual cycle of equatorial sea surface temperature: A coupled general circulation model perspective. *Mon Weather Rev* (in press)
- Dijkstra HA, Neelin JD (1995) Ocean-atmosphere interaction and the tropical climatology. Part II: why the pacific cold tongue is in the east. *J Clim* 8: 1343–1359
- Eckert C, Latif M (1997) Predictability of a stochastically forced hybrid coupled model of El Niño. *J Clim* 10: 1488–1504
- Flato GM, Boer GJ, Lee MG, McFarlane NA, Ramsden D, Reader Mc, Weaver AJ (2000) The Canadian Centre for Climate Modeling and Analysis global coupled model and its climate. *Clim Dyn* 16: 451–467
- Frey H, Latif M, Stockdale T (1997) The coupled GCM ECHO-2 Part I: the tropical Pacific. *Mon Weather Rev* 125: 703–720
- Gordon C, Cooper C, Senior CA, Banks H, Gregory JM, Johns TC, Mitchell JFB, Wood RA (2000) The simulation of SST, sea ice extents and ocean heat transports in a version of the Hadley Centre coupled model without flux adjustments. *Clim Dyn* 16: 147–168
- Ji M, Behringer DW, Leetmaa A (1998) An improved coupled model for ENSO prediction and implications for ocean initialization. Part II: the coupled model. *Mon Weather Rev* 126: 1022–1034
- Kaplan A, Cane MA, Kushnir Y, Clement AC, Blumenthal MB, Rajagopalan B (1997) Analyses of global sea surface temperature 1856–1991. *J Geophys Res* 102: 27 835–27 860
- Kimoto M (2001) Studies of climate variability using general circulation models. In “The Present and Future of Modeling Global Environmental Change—Toward Integrated Modeling—”, Matsuno T (ed), Springer Verlag, in press
- Kimoto M, Shen X-S (1997) Researches of climate variability using general circulation models. Climate System Research Publication Series 291–116. Center for Climate System Research University of Tokyo (in Japanese)
- Kimoto M, Yoshikawa I, Ishii M (1997) An ocean data assimilation system for climate monitoring. *J Meteorol Soc Japan* 75: 471–487
- Knutson TR, Manabe S (1998) Model assessment of decadal variability and trends in the tropical Pacific Ocean. *J Clim* 11: 2273–2296
- Kumar KK, Rajagopalan B, Cane MA (1999) On the weakening relationship between the Indian monsoon and ENSO. *Nature* 284: 2156–2159
- Latif M (1998) Dynamics of interdecadal variability in coupled ocean-atmosphere models. *J Clim* 11: 602–624
- Latif M (2001) Tropical Pacific/Atlantic Ocean interactions at multi-decadal time scales. *Geophys Res Lett* 28: 539–542
- Latif M, Sterl A, Maier-Reimer E, Junge MM (1993) Structure and predictability of the El Niño/Southern Oscillation phenomenon in a coupled ocean-atmosphere general circulation model. *J Clim* 6: 700–708
- Latif M, Roeckner E, Mikolajewicz U, Voss R (2000) Tropical stabilisation of the thermohaline circulation in a greenhouse warming simulation. *J Clim* 13: 1809–1813
- Laurent C, Le Treut H, Li ZX, Fairhead L, Dufresne J-L (1998) The influence of resolution in simulating interannual and interdecadal variability in a coupled ocean – atmosphere GCM. Note IPSL No. 8. Available from IPSL, Paris, France, pp 38
- Li T, Hogan TF (1999) The role of the annual mean climate on seasonal and interannual variability of the tropical Pacific in a coupled GCM. *J Clim* 12: 780–792
- Maier-Reimer E, Mikolajewicz U, Hasselmann K (1993) Mean circulation of the Hamburg LSG model and its sensitivity to the thermohaline surface forcing. *J Phys Oceanogr* 23: 731–757
- Manabe S, Stouffer RJ, Spelman MJ, Bryan K (1991) Transient responses of a coupled ocean-atmosphere model to gradual changes of atmospheric CO₂ Part I: annual mean response. *J Clim* 4: 785–818
- Mechoso, et al (2000) A coupled GCM pilgrimage: From climate catastrophe to ENSO simulations. In: General Circulation Model Development: Past, Present, and Future, Randall DA (ed), Academic Press, pp 539–575
- Mechoso CR, et al (1995) The seasonal cycle over the tropical Pacific in coupled ocean-atmosphere general circulation models. *Mon Weather Rev* 123: 2825–2838
- Meehl GA, Washington WM (1996) El Niño-like change in a model with increased atmospheric CO₂ concentrations. *Nature* 282: 56–60
- Meehl GA, Boer GJ, Covey C, Latif M, Stouffer RJ (2000a) The coupled model intercomparison project (CMIP). *Bull Am Meteorol Soc* 81: 313–318
- Meehl GA, Gent PR, Arblaster JM, Otto-Bliesner BL, Brady EC, Craig A (2000b) Factors that affect the amplitude of El Niño in global coupled climate models. *Clim Dyn* (in press)
- Nagai T, Tokioka T, Endoh M, Kitamura Y (1992) El Niño-Southern Oscillation simulated in an MRI atmosphere-ocean coupled general circulation model. *J Clim* 5: 1202–1233
- Neelin JD, Dijkstra HA (1995) Ocean-atmosphere interaction and the tropical climatology. Part I: the dangers of flux correction. *J Clim* 8: 1325–1342
- Neelin JD, et al (1992) Tropical air-sea interaction in general circulation models. *Clim Dyn* 7: 73–104
- Oberhuber JM (1993) Simulation of the Atlantic circulation with a coupled sea-ice mixed layer-isopycnal general circulation model. Part I: model description. *J Phys Oceanogr* 13: 808–829
- Pacanowski RC (1995) MOM 2 Documentation user's guide and reference manual, GFDL Ocean Technical Report 3
- Parker DE, Jackson M, Horton EB (1995) The GISST 22 sea surface temperature and sea ice climatology. Climate Research Technical Note 63 Hadley Centre, Meteorological Office, Bracknell, UK, pp 35

- Philander SGH (1990) El Niño, La Niña and the Southern Oscillation. Academic Press, San Diego, USA, pp 293
- Power SB, Kleeman R, Tseitkin F, Smith NR (1995) A global version of the GFDL modular ocean model for ENSO studies. BMRC Tech Rep, pp 18
- Power SB, Tseitkin F, Colman RA, Sulaiman A (1998) A coupled GCM for seasonal prediction and climate change research. BMRC Res Rep 66 pp 52
- Roeckner E, Oberhuber JM, Bacher A, Christoph M, Kirchner I (1996) ENSO variability and atmospheric response in a global coupled atmosphere-ocean model. *Clim Dyn* 12: 737–754
- Schopf PS, Suarez MJ (1988) Vacillations in a coupled ocean-atmosphere model. *J Atmos Sci* 45: 549–566
- Sirven J (1996) The equatorial undercurrent in a two layer shallow water model. *J Maf Sys* 9: 171–186
- Sirven J, Vintzileos A (2000) The seasonal cycle in a coupled experiment with an Atmospheric GCM and a two-layer equatorial ocean model. *Clim Dyn* 16: 851–866
- Slingo JM (1999) The Indian summer monsoon and its variability. In: Navarra A (ed) *Beyond El Niño* Springer, Berlin, Heidelberg New York, pp 103–118
- Sperber KR, Palmer TN (1996) Interannual tropical rainfall variability in general circulation model simulations associated with the Atmospheric Model Intercomparison Project. *J Clim* 9: 2727–2750
- Sperber KR, Slingo JM, Annamalai H (2000) Predictability and the relationship between subseasonal and interannual variability during the Asian summer monsoon. *Q J R Meteorol Soc* 126: 2545–2574
- Terray L (1998) Sensitivity of climate drift to atmospheric physical parameterizations in a coupled ocean-atmosphere model. *J Clim* 11: 1633–1658
- Timmermann A, Latif M, Voss R, Grötxner A (1998) Northern Hemisphere interdecadal variability: a coupled air-sea mode. *J Clim* 11: 1906–1931
- Venzke S, Latif M, Villwock A (2000) The coupled GCM ECHO-2 Part II: Indian Ocean response to ENSO. *J Clim* 13: 1371–1383
- Vintzileos A, Delecluse P, Sadourny R (1999a) On the mechanisms in a tropical ocean – global atmosphere coupled general circulation model. Part I: mean state and the seasonal cycle. *Clim Dyn* 15: 43–62
- Vintzileos A, Delecluse P, Sadourny R (1999b) On the mechanisms in a tropical ocean – global atmosphere coupled general circulation model. Part II: interannual variability and its relation to the seasonal cycle. *Clim Dyn* 15: 63–80
- Voss R, Sausen R, Cubasch U (1998) Periodically synchronously coupled integrations with the atmosphere-ocean general circulation model ECHM3/LSG. *Clim Dyn* 14: 249–266
- Wang B, Fang Z (2000) Roles of shortwave radiation forcing on ENSO: A study with an intermediate coupled ocean - atmosphere model. *Climate Dynamics* 16: 677–691
- Washington WM, Meehl GA (1996) High latitude climate change in a global coupled ocean-atmosphere-sea ice model with increased atmospheric CO₂. *J Geophys Res* 101: 12 795–12 801
- Washington WM, Meehl GA, Verplank L, Bettge TW (1994) A world ocean model for greenhouse sensitivity studies: resolution intercomparison and the role of diagnostic forcing. *Clim Dyn* 9: 321–344
- Watanabe M, Kimoto M, Nitta T, Kachi M (1998) A comparison of decadal climate oscillations in the North Atlantic detected in observations and a coupled GCM. *J Clim* 12: 2920–2940
- Webster PJ, Yang S (1992) Monsoon and ENSO: selectively interactive systems. *Q J R Meteorol Soc* 118: 877–926
- White WB (1995) Network design of a global observing system for gyre-scale upper ocean temperature variability. *Prog Oceanogr* 36: 169–217
- Wolff J-O, Maier-Reimer E, Legutke S (1996) The Hamburg Ocean Primitive Equation Model HOPE. DKRZ Tech Report 13 Hamburg pp 103
- Yoshikawa I, Ishii M, Kimoto M (1995) Characteristics of JMA Coupled Ocean-Atmosphere model. Proc Int Workshop on Numerical Prediction of Oceanic Variations, Tokyo 7–11 March 1995, pp 189–194
- Yukimoto S, Endoh M, Kitamura Y, Kitoh A, Motoi T, Noda A, Tokioka T (1996) Interannual and interdecadal variabilities in the Pacific in an MRI coupled GCM. *Clim Dyn* 12: 667–683
- Zebiak SE, Cane MA (1987) A model El Niño Southern Oscillation. *Mon Weather Rev* 115: 2262–2278